Research Article | Vol. 31, No. 23 / 6 Nov 2023 / Optics Express 39213
Optics EXPRESS

High-aspect-ratio dielectric pillar with nanocavity backed by metal substrate in the infrared range

XIAOYUAN LU,[1,*] ANDREA TOGNAZZI,[2,3] ALFONSO C. CINO,[2] COSTANTINO DE ANGELIS,[3,4] GANG XU,[5] TONGYI ZHANG,[6,7] AND DMITRY SHISHMAREV[8]

[1]School of Medical Engineering, Xinxiang Medical University, Xinxiang 453003, China
[2]Department of Engineering, University of Palermo, Palermo, Viale delle scienze ed. 9, 90128, Italy
[3]Istituto Nazionale di Ottica - Consiglio Nazionale delle Ricerche (INO-CNR), Brescia, Via Branze 45, 25123, Italy
[4]Department of Information Engineering, University of Brescia, Brescia, Via Branze 38, 25123, Italy
[5]School of Optical and Electronical Information, Huazhong University of Science and Technology, Wuhan 430074, China
[6]State Key Laboratory of Transient Optics and Photonics, Xi'an Institute of Optics and Precision Mechanics, Chinese Academy of Sciences, Xi'an 710119, China
[7]University of Chinese Academy of Sciences, Beijing 100049, China
[8]John Curtin School of Medical Research, The Australian National University, ACT 2601, Australia
[*]luxy@xxmu.edu.cn

Abstract: We investigated absorption and field enhancements of shallow nanocavities on top of high-aspect-ratio dielectric pillars in the infrared range. The structure includes a high-aspect-ratio nanopillar array of high refractive index, with nano-cavities on top of the pillars, and a metal plane at the bottom. The enhancement factor of electric field intensity reaches 3180 in the nanocavities and peak absorption reaches 99%. We also investigated the finite-size effect of the presented structure to simulate real experiments. Due to its narrow absorption bandwidth 3.5 nm, it can work as a refractive index sensor with sensitivity 297.5 nm/RIU and figure of merit 85. This paves the way to directly control light field at the nanoscales in the infrared light range. The investigated nanostructure will find applications in multifunctional photonics devices such as chips for culturing cells, refractive index sensors, biosensors of single molecule detection and nonlinear sensors.

1. Introduction

In recent years, metasurfaces [1] have been investigated in plenty of applications including sensors [2], energy harvesting devices [3], and high resolution imaging [4], due to their ability to mold the electromganetic field at the nanoscale [5]. Plasmonic metasurfaces are particularly suitable for sensing applications since they allow to achieve high field enhancements and sharp spectral features [6–8]. However, the intrinsic losses of metals in the visible region [9] hinder the development of plasmonic nanodevices in that region due to broader resonances, which are more challenging to employ for refractive index sensing [10]. To reduce the detrimental effects caused by losses in metals, dielectric nanostructures have been investigated due to their low intrinsic losses and tunability [11–13]. Dielectric resonators enhances the electromagnetic field inside the device and might be considered less sensitive to the surrounding medium. However, it is possible to exploit sharp resonances, which are extremely vulnerable to environmental perturbations, such as bound states in the continuum or exceptional points, to build competitive optical sensors

#506208 https://doi.org/10.1364/OE.506208
Journal © 2023 Received 18 Sep 2023; revised 24 Oct 2023; accepted 25 Oct 2023; published 2 Nov 2023

Optics EXPRESS

[14–17], guiding light direction [18], and improving radiation efficiency [19]. Metallic mirrors or metal films are introduced in the dielectric structures to further improve field enhancement, light funneling, absorption and directionality [20]. These structures have constituted basic elements for developing new spectroscopic tools based on surface electric field enhancement effects in addition to plasmonic nanostructures [21,22].

In this framework, hybrid metasurfaces allow to merge the advantages of dielectric and plasmonic devices to obtain greater flexibility in shaping the radiation pattern at both the fundamental and second harmonic frequency [23], and improve sensing performances [24]. In particular, the use of nano-voids and nano-slits were proved to be suitable geometrical implementations to obtain large field enhancement in both dielectric and hybrid structures [8,25].

High-aspect ratio (HAR) nanopillars were already employed in culturing cells [26,27] and tailoring chemical processes [28] by shaping the local electric field. Here, we propose a hybrid nonlocal metasurface for optical sensing, composed by HAR dielectric nanopillars on a metallic substrate, featuring a nano-slit on the top side to enhance the electric field localization and obtain narrow absorption spectral features. Finally, we present a comprehensive study to unveil the optical response dependence of a HAR hybrid nonlocal metasurface on the geometrical parameters and finite size effects, which are relevant when considering the fabrication of high-quality factor devices [29,30]. This study further confirms the nonlocal nature of the ongoing optical response. The tunability of the high electric field enhancement, performed by changing geometrical parameters, is exploited to perform refractive index sensing at multiple wavelengths in the third telecommunication window, and highlight potential use as a substrate design for culturing cells.

2. Model and methods

Figure 1 reports the periodic metasurface under study. The unit cell, with periodicity (p), is composed by an infinite dielectric pillar with width (w) and height (h) extending along the z-direction. A small nano-slit on the top, with width (δ) and depth (l), is present. The array lies on a metallic film with thickness (L), which is introduced to improve the electric field enhancement [31], and a glass substrate. The periodic structure can be fabricated by performing wet-transfer of dielectric metasurfaces onto a plasmonic mirror [32] or by evaporating a metallic layer over which amorphous silicon is deposited by plasma-enhanced chemical vapor deposition. In the latter case, the periodic structure is realized by an additional step involving SiO_2 nanodisks fabricated with electron-beam lithography and reactive ion etching [33]. In both cases, the nano-slit on top of the resonators can be realized by a two-step e-beam lithography process [34,35]. We consider a plane wave impinging at normal incidence with wavevector (k_y) and polarized along the x-axis.

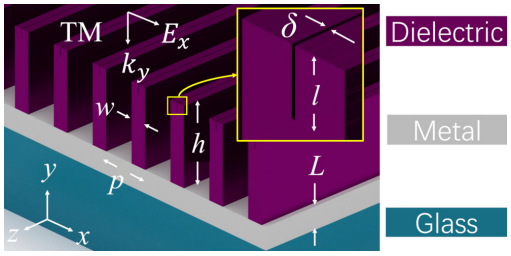

Fig. 1. Schematic of the hybrid metasurface composed by a periodic array of resonant dielectric pillars (purple) with a nano-slit on top lying on a metal film (grey) and glass substrate (light-blue). E_x represents electric field of the transverse magnetic (TM) polarized incident light and k_y represents the direction of propagation.

Optics EXPRESS

We employ Comsol Multiphysics to perform finite element method simulations in the frequency domain. The computational burden of the problem is drastically reduced by exploiting the periodicity and the symmetries of the problem, which allow to simulate only the *xoy* cross section of a single unit cell (or a finite number of resonators in the case of the finite structure). We consider a plane wave at normal incidence with TM polarization (see Fig. 1). The refractive index of aluminum is taken from [36], and the dielectric constant of silicon is taken from [37]. We set the maximum and minimum mesh element size to 20 nm and 0.1 nm, respectively. We define the electric and magnetic field enhancement in the nano-slit as:

$$F_{\mathrm{e}} = \frac{\int |E|^2 \mathrm{d}S}{\int |E_0|^2 \mathrm{d}S} \qquad \text{and} \qquad F_{\mathrm{m}} = \frac{\int |H| \mathrm{d}S}{\int |H_0| \mathrm{d}S}, \tag{1}$$

where E and H are the calculated electric and magnetic fields, E_0 and H_0 are the incident electric and magnetic fields and the integral is performed over the cross sectional area of the nano-slit of the dielectric structure.

3. Results

3.1. Field enhancement in single HAR pillar

We begin our analysis considering a single isolated HAR pillar electromagnetic field distribution and field enhancement spectra. These elements are fundamental building blocks to understand the enhancement mechanism of the periodic metasurface. In Fig. 2(a), we report absorption (A), F_e, and F_m as a function of the wavelength. Three peaks of A at the wavelengths λ_1 = 1411.2 nm, λ_2 = 1575.5 nm, and λ_3 = 1782.7 nm are present, while electric field enhancement has three peaks at 1405.6 nm, 1574.3 nm, and 1781.3 nm. Additionally, magnetic field enhancement has three peaks are at 1411.2 nm, 1580 nm, and 1794 nm. Figure 2(a) (bottom) shows the far field pattern of the single pillar at the three resonant wavelengths, which present a main lobe along the normal direction and multiple side lobes. In Figs. 2(b-g), we report the electric (top row) and magnetic (bottom row) field distribution at λ_1, λ_2 and λ_3, which clearly show the contribution of high order Mie-multipoles. Although high-order multipoles usually lead to higher field enhancement, in the following we show that it is possible to further enhance F_e and F_m by introducing a periodicity.

3.2. Absorption, electric and magnetic field enhancement spectra

Remarkable optical sensing performances are often related to sharp spectral resonances, which can be achieved by properly arranging single resonators. Thus, we report in Fig. 3 the F_e, F_m and A spectra, under TM excitation, to unveil the electromagnetic field localization mechanism in a metasurface composed by HAR pillars.

The absorption spectrum in Fig. 3 shows four resonant peaks at λ_1=1408.4 nm, λ_2=1560.8 nm, λ_3=1761.8 nm, and λ_4=1868.3 nm in the range from 1.4 μm to 2.0 μm. From the spectrum curves, there is a superposition of A, F_e, and F_m spectra at λ_2, but slight deviations at λ_1 and large deviations at λ_3 for peaks of F_e and F_m with respect to A peaks. In the field enhancement spectra, the maximum F_e of 1738.8 and the maximum F_m of 18.9 are at λ_2, which is significantly sharper than the other three resonances. Additionally, the absorption values at λ_2 and λ_4 are far larger than those at λ_1 and λ_3. The F_m peak of λ_3 is at 1781.3 nm, which is 20 nm red shifted with respect to A resonant wavelength. Differently, at the resonant wavelength λ_4, electric field and magnetic field are not much enhanced in the nanocavity compared to the other three resonance, since F_e = 9.6 and F_m= 0.8. The enhancement factor F_e is 10.9 at the wavelength 1872.7 nm and F_m is 2.2 at the wavelength 1896.7 nm, which are not the resonant wavelength. These can be explained by the enhanced field distributions at the resonant wavelengths.

Optics EXPRESS

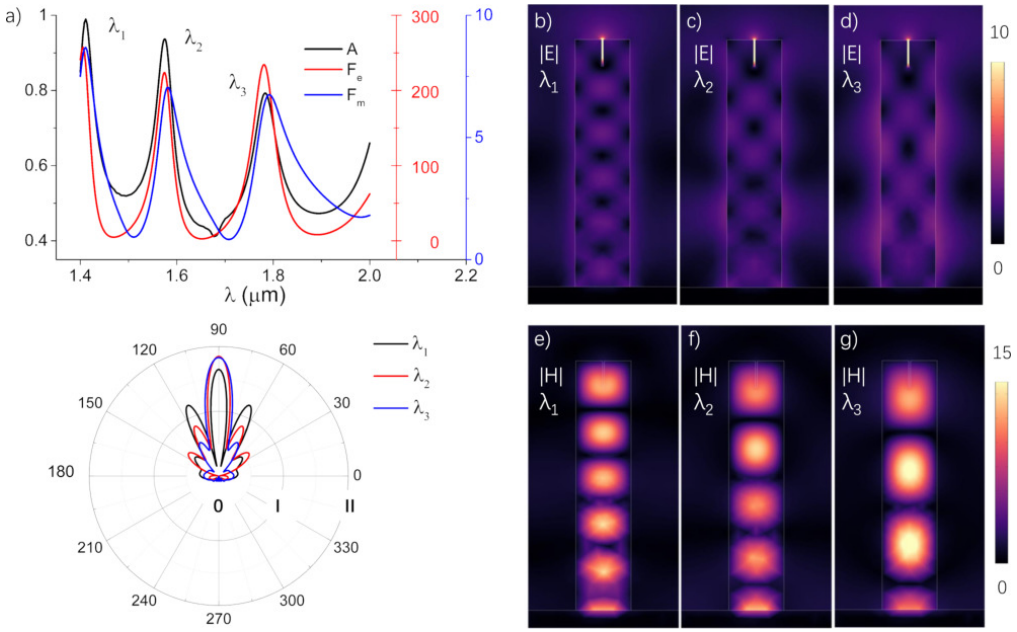

Fig. 2. (a) Absorption (black), F_{e} (red), F_{m} (blue) spectra (top), and radiation pattern (bottom) of a single nanoantenna for TM polarized light. Absorption resonant wavelengths are $\lambda_1 = 1411.2$ nm, $\lambda_2 = 1575.5$ nm, and $\lambda_3 = 1782.7$ nm, while peak values of F_{e} are at: 1405.6 nm, 1574.3 nm, and 1781.3 nm. For peaks of F_e, 257 at λ_1, 223 at λ_2, 234 at λ_3. For peaks of F_m, 8.7 at λ_1, 7 at λ_2, 6.7 at λ_3. In (a. bottom), I and II represent 1.75×10^{-3} and 3.50×10^{-3}, respectively. (b-d) Distributions of normalized electric field $|E|$ and (e-g) magnetic amplitude $|H|$ at the three wavelengths: (b)(e) λ_1, (c)(f) λ_2, and (d)(g) λ_3. Geometrical parameters: $w = 300$ nm, $\delta = 10$ nm, $h = 1400$ nm, $l = 150$ nm, $p = 845$ nm, and the whole structure is in the air.

In Fig. 3, we report the electric (b-e) and magnetic (f-i) field enhancements to unveil the nature of the above mentioned spectral features. The first and third peaks at λ_1 and λ_3 present an increased electric and magnetic field localization inside the dielectric structure, showing that they originate from high order magnetic multipolar modes perpendicular to the incident electric field [11]. Whereas the second and fourth peaks at λ_2 and λ_4 present electric field enhancement not only in the pillar but also in the domain close to the interface of silicon and the surrounding. As the field distribution suggests, the peak at λ_4 might be related to a boundary mode, while the peak at λ_2 originates from high-Q collective Mie-type modes and quasi-BIC modes leading to their hybridization [38]. The nonlocal nature of the mode is confirmed by the finite size dependence of the mode at λ_2. As the field distribution suggests, the peaks at λ_1 and λ_3 are related to resonances of the isolated pillar (see Figs. 2(e) and (g)). The periodicity further enhances the electric and magnetic field inside the resonators by closing the radiation channels along the directions of the side lobes (see Fig. 2(a) bottom) [39]. Figures 3(f-i) show that the nodes and antinodes of the magnetic field distributions are with different heights for the resonant wavelengths, which is the main course of discrepancy among the peak values. The top antinode of magnetic field $|H|$ distribution of λ_1 is located a little higher than that of the resonant wavelength λ_2. For the resonant wavelength λ_4, electric field enhancement F_e is not notable because enhanced electric field components are close to the three interfaces including external walls of the nanopillar (nanopillar-air, nanopillar-metal and air-metal), whereas antinode of magnetic field distribution is far from the nanocavity.

Optics EXPRESS

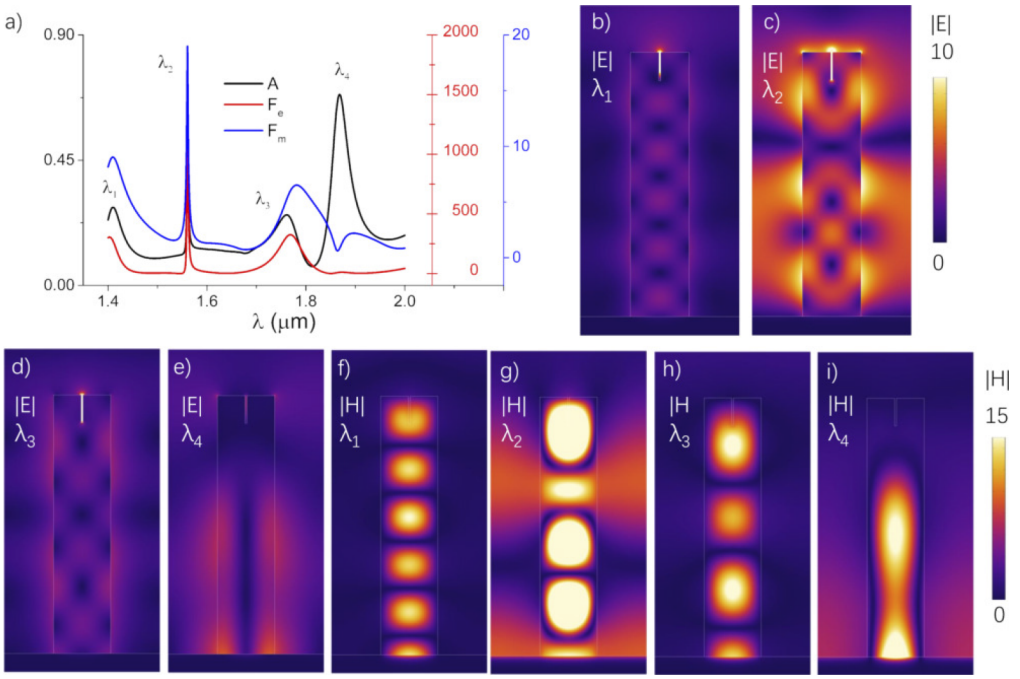

Fig. 3. (a) Absorption (A), electric field enhancement factor (F_e), and magnetic field enhancement factor (F_m) spectra of the HAR structure at normal incident TM polarized light. The absorption peaks are at λ_1 = 1408.4 nm, λ_2 = 1560.8 nm, λ_3 = 1761.3 nm, and λ_4 = 1868.3 nm. F_e reaches values of 305.7 at λ_1, 1738.8 at λ_2, 324.8 at λ_3, 10.9 at λ_4. F_m reaches values of 9 at λ_1, 18.9 at λ_2, 6.5 at λ_3, 2.2 at λ_4. (b-e) Distributions of normalized electric field intensity $|E|$ (top row) and magnetic field $|H|$ (bottom row) of the presented nanostructure. Structural parameters: w = 300 nm, δ = 10 nm, h = 1400 nm, l = 150 nm, p = 845 nm. The whole structure is in air.

3.3. *Tunability of the geometrical parameters*

Structural parameters are key elements for photonic response of nanostructures. Although nanofabrication techniques dramatically improved in the last two decades, fabrication tolerances should be accounted. Thus, we investigate geometrical dependence of the optical properties of the presented HAR structure. Figure 4 shows tunable properties of electric field enhancement for the presented HAR structure. When the array period p is varied from 700 nm to 1250 nm, the resonant wavelength redshifts, as shown in Fig. 4(a). Figure 4(b) shows that the enhancement spectra are influenced by the length l of the nano-slit when it is increased from 100 nm to 200 nm. The resonant wavelength blue shifts while the nanocavity length increases. In Fig. 4(c), the resonant wavelength redshifts when the nanocavity width δ increases from 5 nm to 30 nm; peak absorption value sharply reduces when the nanocavity width is larger than 20 nm. We obtained field enhancement F_e = 3180 and A = 99% at the wavelength 1558 nm while p = 845 nm, δ = 5 nm, l = 150 nm, and h = 1400 nm. We fix the wavelength at 1550 nm while the width and period of the nanocavity are respectively varied from 3 nm to 10 nm and 770 nm to 820 nm. Figure 4(d) shows that peak value of light intensity enhancement reaches 2270 at p = 800 nm and δ = 3 nm. The length of the nano-slit does not affect the width of the narrow resonant peak, while F_e decreases when the width of the nano-slit increases.

Optics EXPRESS

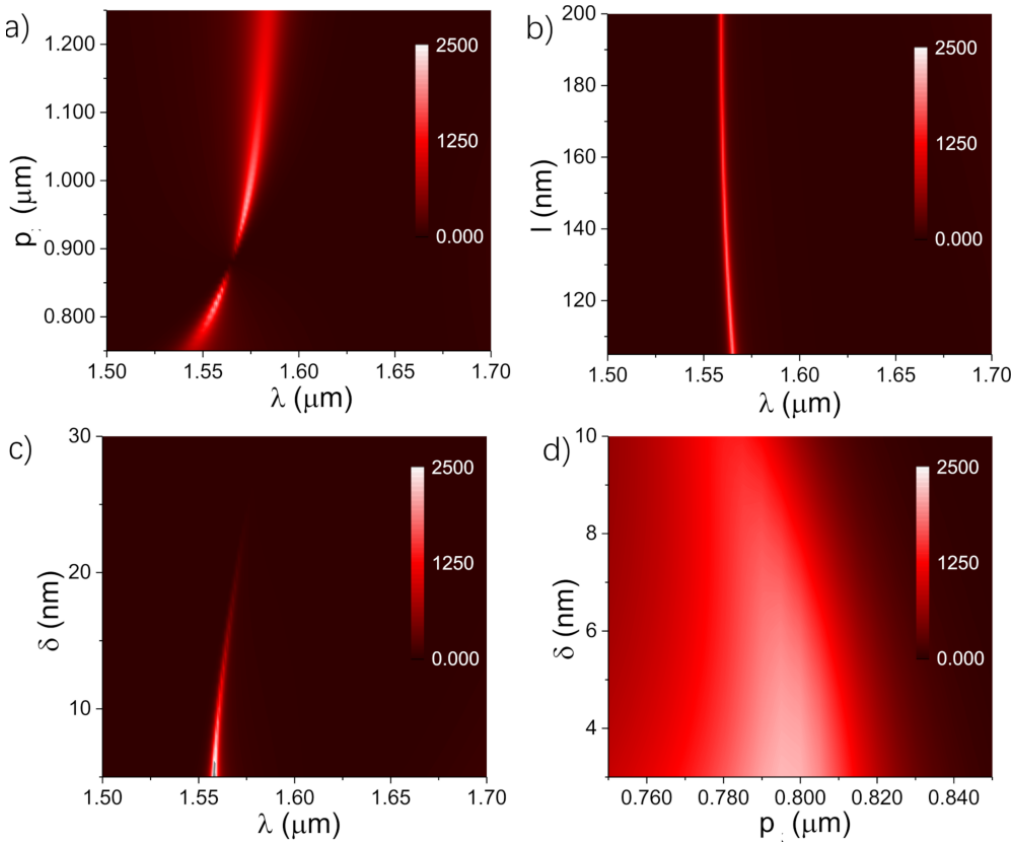

Fig. 4. F_e as a function of the wavelength and (a) period, (b) nano-slit length, (c) nano-slit width for TM polarized incident light. (d) F_e as a function of different slit width and period at fixed incident wavelength 1550 nm.

4. Finite-size effects

Previously, we assumed the structure to be infinitely extended along the x-direction. However, in real experiments, these kinds of periodic structures, such as metasurface, metamaterials, and photonic crystals, always have a finite number of unit cells, which bring finite size effects into play [30,40]. In [40], the authors reported that finite size effects of systems lead to counter-intuitive behavior of competition between multiple loss channels including dissipation, intentional out coupling of coherent radiation, and leakage from the edges of finite systems. Here, we investigated the spectral response of finite-size periodic arrays to evaluate the correctness of our approximation to an infinite structure and provide a guideline to understand the minimum size to observe sizable increase of absorption due to nonlocal effects. To simulate the real experiment in air, we set the length of a chip along the x axis to 60 μm and perfectly matched layers along the x-axis. Figure 5(a) shows that for less than 15 unit cells, no sizable absorption enhancement is present. The inset of Fig. 5(a) shows the narrow part of the spectra related to λ_2. We note that as the number of unit cells increases, the resonances blue shift and the spectra converge to the one of the infinite structure. We also note that when the number of unit cells is larger than 30, the variation of the resonant position is almost negligible when adding additional unit cells. Indeed, Fig. 5(b) shows the resonant wavelengths λ_2 and λ_4 are blue shifted with increasing number of cells. For example, λ_2 changes from 1567.5 nm to 1560.8 nm, and λ_4 shifts from 1905.2 nm to 1869.3 nm.

Optics EXPRESS

5. Sensing performance

Now, we investigate the sensing performance of the presented HAR metasurface when it is operated as a refractive index sensor. We assume the surrounding to be an aqueous solution, which has a typical refractive index in the range 1.312-1.352 [41]. Figure 6 shows that the resonant wavelengths λ_2 and λ_4 linearly depend on the environment refractive index. As shown in Fig. 6, when the refractive index is changed, the resonant wavelengths redshift from 1418.2 nm to 1430.1 nm for λ_2 and from 1938 nm to 1948 nm for λ_4. The variation of 0.04 in the refraction index induces shifts of the resonant wavelengths $\Delta\lambda_2$ = 11.9 nm and $\Delta\lambda_4$ = 10 nm. Based on the definition of sensitivity (S) [41], S is 297.5 nm/RIU and 250 nm/RIU for λ_2 and λ_4, respectively. Following the definition of figure of merit (FoM) [41], FoM is 85 with a FWHM of 3.5 nm at λ_2 and FoM is 8.3 with a FWHM of 30.2 nm at λ_4. The results show that although its sensitivity is smaller, compared to other metal-dielectric-metal structures [6,41], the FWHM of the considered resonances is far narrower than that of other metal-dielectric-metal structures. Thus, the presented HAR structure has larger FoM in the near infrared light range. Moreover, we proposed a structure working at multiple wavelengths with comparable sensing performance, which allows to simultaneously cross check the resonance shift and improve the reliability of our device. Here, we did not evaluate sensing performance of the other resonant wavelengths λ_1 and λ_3 because the spectrum curve presents weak absorption at those wavelengths.

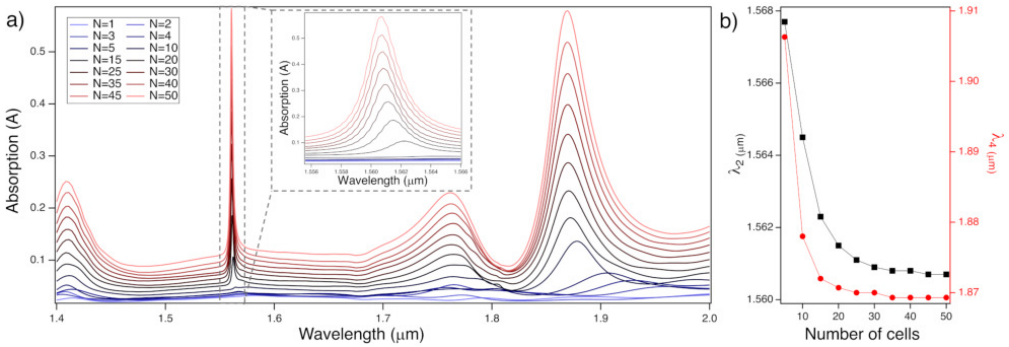

Fig. 5. (a) Absorption spectrum of the finite-size nanostructure array consisting of a different number of unit cells. The device size is 60 μm wide. (b) Resonant wavelengths λ_2 (black, left) and λ_4 (red, right) as a function of the number of unit cells. Geometrical parameters: w = 300 nm, δ = 10 nm, h = 1400 nm, l = 150 nm, p = 845 nm. The whole structure is in the air.

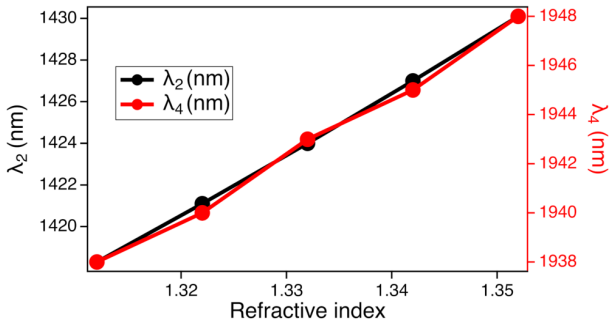

Fig. 6. Resonant wavelengths λ_2 (black, left) and λ_4 (red, right) as a function of the refractive index in the surrounding.

Optics EXPRESS

6. Conclusion

In summary, we numerically investigated a hybrid metasurfaces based on HAR dielectric pillar structure, through which we obtain the multiple narrowband absorption peaks in the spectrum. The local electric field intensity is enhanced up to 3 orders of magnitude for the incident light with TM polarization. We performed feasibility study by investigating the absorption and field enhancement as a function of the geometrical parameters and accounting for finite size effects. We show that HAR nanopillar structures are suitable to perform refractive index sensing at multiple wavelength, reaching sensitivities up to 297.5 nm/RIU and figure of merit of 85. The possibility to perform sensing at multiple wavelengths with comparable efficiencies allows to improve the reliability of measurements. Our results provide insight in the design of refractive index sensors based on compact photonic platforms.

Funding. Horizon 2020 Framework Programme (899673); Ministero dell'Università e della Ricerca (2020EY2LJT_002); National Health and Medical Research Council (GNT1173015); National Natural Science Foundation of China (62171443, 62275097); China Scholarship Council (202008410575).

Acknowledgement. A. Tognazzi acknowledges the financial support from the European Union through "FESR o FSE, PON Ricerca e Innovazione 2014-2020 - DM 1062/2021" and the University of Palermo through "Fondo Finalizzato alla Ricerca di Ateneo 2023 (FFR2023)". Dmitry Shishmarev acknowledges the financial support from the National Health and Medical Research Council of Australia (GNT1173015). Gang Xu, Tongyi Zhang, and Xiaoyuan Lu acknowledge the financial support from the National Natural Science Foundation of China (Grant Nos. 62275097 and 62171443) and the China Scholarship Council (Grant No. 202008410575).

Disclosures. The authors declare no conflicts of interest.

Data availability. The authors confirm that the data supporting the findings of this study are available within the article.

References

1. H. Chen, A. J. Taylor, and N. Yu, "A review of metasurfaces: physics and applications," Rep. Prog. Phys. **79**(7), 076401 (2016).
2. R. Chikkaraddy, B. De Nijs, F. Benz, *et al.*, "Single-molecule strong coupling at room temperature in plasmonic nanocavities," Nature **535**(7610), 127–130 (2016).
3. Z. Li, E. Palacios, S. Butun, *et al.*, "Omnidirectional, broadband light absorption using large-area, ultrathin lossy metallic film coatings," Sci. Rep. **5**(1), 15137 (2015).
4. P. Bouchal, P. Dvořk, J. Babocký, *et al.*, "High-resolution quantitative phase imaging of plasmonic metasurfaces with sensitivity down to a single nanoantenna," Nano Lett. **19**(2), 1242–1250 (2019).
5. J. J. Baumberg, J. Aizpurua, M. H. Mikkelsen, *et al.*, "Extreme nanophotonics from ultrathin metallic gaps," Nat. Mater. **18**(7), 668–678 (2019).
6. X. Lu and J. Lin, "Field enhancement of a metal grating with nanocavities and its sensing applications," J. Opt. **19**(5), 055004 (2017).
7. M. Bora, B. J. Fasenfest, E. M. Behymer, *et al.*, "Plasmon resonant cavities in vertical nanowire arrays," Nano Lett. **10**(8), 2832–2837 (2010).
8. J. Le Perchec, "On the giant enhancement of light in plasmonic or all-dielectric gratings containing nano-voids," Opt. Lett. **44**(3), 590–593 (2019).
9. S. V. Boriskina and L. Dal Negro, "Multiple-wavelength plasmonic nanoantennas," Opt. Lett. **35**(4), 538–540 (2010).
10. N. Bosio, H. Šípová-Jungová, N. O. Länk, *et al.*, "Plasmonic versus all-dielectric nanoantennas for refractometric sensing: A direct comparison," ACS Photonics **6**(6), 1556–1564 (2019).
11. R. M. Bakker, D. Permyakov, Y. Yu, *et al.*, "Magnetic and electric hotspots with silicon nanodimers," Nano Lett. **15**(3), 2137–2142 (2015).
12. M. Darvishzadeh-Varcheie, M. Kamandi, M. Albooyeh, *et al.*, "Optical magnetic field enhancement at nanoscale: a nanoantenna comparative study," Opt. Lett. **44**(20), 4957–4960 (2019).
13. P. Franceschini, A. Tognazzi, G. Finco, *et al.*, "Nonlocal resonances in pedestal high-index-contrast metasurfaces based on a silicon-on-insulator platform," Appl. Phys. Lett. **123**(7), 071701 (2023).
14. J. Cambiasso, G. Grinblat, Y. Li, *et al.*, "Bridging the gap between dielectric nanophotonics and the visible regime with effectively lossless gallium phosphide antennas," Nano Lett. **17**(2), 1219–1225 (2017).
15. A. Tognazzi, D. Rocco, M. Gandolfi, *et al.*, "High quality factor silicon membrane metasurface for intensity-based refractive index sensing," Optics **2**(3), 193–199 (2021).
16. J. Wiersig, "Review of exceptional point-based sensors," Photonics Res. **8**(9), 1457 (2020).
17. W. Tuxbury, R. Kononchuk, and T. Kottos, "Non-resonant exceptional points as enablers of noise-resilient sensors," Commun. Phys. **5**(1), 210 (2022).

Optics EXPRESS

18. N. Rivera, C. W. Hsu, B. Zhen, *et al.*, "Controlling directionality and dimensionality of radiation by perturbing separable bound states in the continuum," Sci. Rep. **6**(1), 33394 (2016).
19. A. Barreda, S. Hell, M. Weissflog, *et al.*, "Metal, dielectric and hybrid nanoantennas for enhancing the emission of single quantum dots: A comparative study," J. Quant. Spectrosc. Radiat. Transfer **276**, 107900 (2021).
20. Á. Barreda, F. Vitale, A. E. Minovich, *et al.*, "Applications of hybrid metal-dielectric nanostructures: State of the art," Adv. Photonics Res. **3**(4), 2100286 (2022).
21. P. Albella, M. A. Poyli, M. K. Schmidt, *et al.*, "Low-loss electric and magnetic field-enhanced spectroscopy with subwavelength silicon dimers," J. Phys. Chem. C **117**(26), 13573–13584 (2013).
22. M. Caldarola, P. Albella, E. Cortés, *et al.*, "Non-plasmonic nanoantennas for surface enhanced spectroscopies with ultra-low heat conversion," Nat. Commun. **6**(1), 7915 (2015).
23. V. F. Gili, L. Ghirardini, D. Rocco, *et al.*, "Metal–dielectric hybrid nanoantennas for efficient frequency conversion at the anapole mode," Beilstein J. Nanotechnol. **9**, 2306–2314 (2018).
24. X. Lu, T. Zhang, R. Wan, *et al.*, "Numerical investigation of narrowband infrared absorber and sensor based on dielectric-metal metasurface," Opt. Express **26**(8), 10179–10187 (2018).
25. Y. Yang, V. A. Zenin, and S. I. Bozhevolnyi, "Anapole-assisted strong field enhancement in individual all-dielectric nanostructures," ACS Photonics **5**(5), 1960–1966 (2018).
26. J. Harberts, K. Bours, M. Siegmund, *et al.*, "Culturing human iPSC-derived neural progenitor cells on nanowire arrays: mapping the impact of nanowire length and array pitch on proliferation, viability, and membrane deformation," Nanoscale **13**(47), 20052–20066 (2021).
27. V. Gautam, S. Naureen, N. Shahid, *et al.*, "Engineering highly interconnected neuronal networks on nanowire scaffolds," Nano Lett. **17**(6), 3369–3375 (2017).
28. M. Holgado, C. Barrios, F. Ortega, *et al.*, "Label-free biosensing by means of periodic lattices of high aspect ratio SU-8 nano-pillars," Biosens. Bioelectron. **25**(12), 2553–2558 (2010).
29. F. Gambino, M. Giaquinto, A. Ricciardi, *et al.*, "A review on dielectric resonant gratings: Mitigation of finite size and gaussian beam size effects," Results in Optics **6**, 100210 (2022).
30. L. Ciarella, A. Tognazzi, F. Mangini, *et al.*, "Finite-size and illumination conditions effects in all-dielectric metasurfaces," Electronics **11**(7), 1017 (2022).
31. A. Dhibi, "A comparative study of surface plasmon resonance sensors by using doped-silicon grating structure on doped silicon and aluminum film," Phys. Scr. **94**(10), 105602 (2019).
32. Y. Zhang, Z. Zhang, C. Xu, *et al.*, "Precisely constructing hybrid nanogap arrays via wet-transfer of dielectric metasurfaces onto a plasmonic mirror," Opt. Express **31**(21), 34280 (2023).
33. L. Xu, M. Rahmani, K. Z. Kamali, *et al.*, "Boosting third-harmonic generation by a mirror-enhanced anapole resonator," Light: Sci. Appl. **7**(1), 44 (2018).
34. C. Gigli, G. Marino, A. Artioli, *et al.*, "Tensorial phase control in nonlinear meta-optics," Optica **8**(2), 269 (2021).
35. A. Tognazzi, K. I. Okhlopkov, A. Zilli, *et al.*, "Third-harmonic light polarization control in magnetically resonant silicon metasurfaces," Opt. Express **29**(8), 11605 (2021).
36. K. M. McPeak, S. V. Jayanti, S. J. P. Kress, *et al.*, "Plasmonic films can easily be better: rules and recipes," ACS Photonics **2**(3), 326–333 (2015).
37. D. T. Pierce and W. E. Spicer, "Electronic structure of amorphous Si from photoemission and optical studies," Phys. Rev. B **5**(8), 3017–3029 (1972).
38. K. I. Okhlopkov, A. Zilli, A. Tognazzi, *et al.*, "Tailoring third-harmonic diffraction efficiency by hybrid modes in high-q metasurfaces," Nano Lett. **21**(24), 10438–10445 (2021).
39. S. Joseph, S. Pandey, S. Sarkar, *et al.*, "Bound states in the continuum in resonant nanostructures: an overview of engineered materials for tailored applications," Nanophotonics **10**(17), 4175–4207 (2021).
40. S. Droulias, T. Koschny, and C. M. Soukoulis, "Finite-size effects in metasurface lasers based on resonant dark states," ACS Photonics **5**(9), 3788–3793 (2018).
41. N. Liu, M. Mesch, T. Weiss, *et al.*, "Infrared perfect absorber and its application as plasmonic sensor," Nano Lett. **10**(7), 2342–2348 (2010).